Magnetic Resonance in Medical Sciences, Vol. 4, No. 1, p. 35–42, 2005

MAJOR PAPER

ADC Mapping of Benign and Malignant Breast Tumors

Reiko WOODHAMS[1]*, Keiji MATSUNAGA[1], Shinichi KAN[1], Hirofumi HATA[1], Masanori OZAKI[4], Keiichi IWABUCHI[2], Masaru KURANAMI[3], Masahiko WATANABE[3], and Kazushige HAYAKAWA[1]

[1]*Department of Radiology,* [2]*Department of Pathology,* [3]*Department of Surgery, Kitasato University School of Medicine*
[4]*Department of Medical Engineering and Technology, Kitasato University School of Allied Health Science*
1-15-1 Kitasato, Sagamihara, Kanagawa 228-8555, Japan
(Received March 10, 2005; Accepted May 18, 2005)

Purpose: The purpose of this study was to investigate the utility of diffusion-weighted imaging (DWI) and the apparent diffusion coefficient (ADC) value in differentiating benign and malignant breast lesions and evaluating the detection accuracy of the cancer extension.

Materials and Methods: We used DWI to obtain images of 191 benign and malignant lesions (24 benign, 167 malignant) before surgical excision. The ADC values of the benign and malignant lesions were compared, as were the values of noninvasive ductal carcinoma (NIDC) and invasive ductal carcinoma (IDC). We also evaluated the ADC map, which represents the distribution of ADC values, and compared it with the cancer extension.

Results: The mean ADC value of each type of lesion was as follows: malignant lesions, $1.22 \pm 0.31 \times 10^{-3}$ mm^2/s; benign lesions, $1.67 \pm 0.54 \times 10^{-3}$ mm^2/s; normal tissues, $2.09 \pm 0.27 \times 10^{-3}$ mm^2/s. The mean ADC value of the malignant lesions was statistically lower than that of the benign lesions and normal breast tissues. The ADC value of IDC was statistically lower than that of NIDC. The sensitivity of the ADC value for malignant lesions with a threshold of less than 1.6×10^{-3} mm^2/s was 95% and the specificity was 46%. A full 75% of all malignant cases exhibited a near precise distribution of low ADC values on ADC maps to describe malignant lesions. The main causes of false negative and underestimation of cancer spread were susceptibility artifact because of bleeding and tumor structure. Major histologic types of false-positive lesions were intraductal papilloma and fibrocystic diseases. Fibrocystic diseases also resulted in overestimation of cancer extension.

Conclusions: DWI has the potential in clinical appreciation to detect malignant breast tumors and support the evaluation of tumor extension. However, the benign proliferative change remains to be studied as it mimics the malignant phenomenon on the ADC map.

Keywords: ***breast cancer, breast MRI, DWI, fibrocystic disease, susceptibility artifact***

Introduction

The latest advancements in MRI (magnetic resonance imaging) technology have greatly expanded the utility of diffusion-weighted imaging (DWI) in the examination of various organs and diagnosis of various disorders.[1-4] DWI has already been applied in the important clinical use of diagnosis of brain ischemia and for differentiating brain abscess from metastatic brain tumor.[5,6] Moreover several studies have revealed the usefulness of DWI in characterizing brain lesions and tumors of the liver, pancreas, and ovary.[7-12] The greatest advantage of DWI in the diagnosis of neoplasm is that DWI reflects the biological character of the tissue. Furthermore, an enhancing material is not necessary. DWI is already achieving the stage of clinical application.

The use of DWI for breast cancer diagnosis is also recently being considered in clinical application.[3,13-15] Some authors showed lower ADC values for breast cancer compared with normal breast tissue. Y. Kuroki et al. also showed the utility of

*Corresponding author, Phone: +81-42-778-8453, E-mail: reiko99@db3.so-net.ne.jp

Table 1. Distribution of mean ADC values in histologic types of benign lesions

Benign Lesions	n	Mean ADC value (10^{-3} mm^2/s)
Fibrocystic disease	8	1.65 ± 0.28
Intraductal papilloma	6	1.32 ± 0.15
No evidence of malignancy	3	2.50 ± 0.44
Phyllodes benign	3	2.00 ± 0.45
Fibroadenoma	2	1.10 ± 0.23
Atypical hyperplasia	1	1.7
Granuloma (after plastic surgery)	1	0.7
Total	24	

Table 2. Distribution of mean ADC values in histologic types of breast cancer

Malignant Lesions	n	Mean ADC value (10^{-3} mm^2/s)
IDC		
Solid tubular Ca	43	1.16 ± 0.26
Papillotubular Ca	38	1.17 ± 0.29
Scirrhous Ca	34	1.17 ± 0.26
Lobular Ca	11	1.07 ± 0.26
Malignant Phyllodes	3	1.67 ± 0.59
Medullary Ca	2	1.05 ± 0.28
Invasive micropapillary Ca	2	1.15 ± 0.21
SCC	2	1.3
Mucinous Ca	2	1.75
Adenoid cystic Ca	1	1.0
NIDC or predominant NIDC		
DCIS	27	1.36 ± 0.20
Intracystic papillary Ca	2	2.6 ± 0.14
Total	167	

parallel imaging for breast DWI and displayed the significant difference between the ADC of malignant tumor and benign tumor.[15] Y. Guo et al. interpreted the correlation between cell density and ADC value and showed the inverse proportion between them.[3]

We investigate the usefulness of DWI for qualitative diagnosis of the breast and verify the sensitivity, specificity, and accuracy of DWI for breast cancer. We also evaluate the efficacy of the ADC map for assessing cancer extension.

Materials and Methods

Subjects: The subjects comprised 190 patients with a total of 191 lesions who had undergone MRI for breast examination due to tumor palpability, bloody secretion, calcification on mammography, and follow up after plastic surgery. All patients were female and aged between 14 and 88 years (mean age: 53 years). All patients underwent surgical resection and received definite pathological diagnosis.

Histological detail: Findings were 24 benign lesions, including 7 ductal hyperplasia, 1 sclerosing adenosis, 6 intraductal papilloma, 1 atypical ductal hyperplasia, 3 benign phyllodes tumor, 2 fibroadenoma, 1 granuloma, and 3 with no evidence of abnormality (Table 1). Malignant lesions totaled 167, including 43 solid-tubular carcinoma, 38 papillotubular carcinoma, 34 scirrhous carcinoma, 27 ductal carcinoma in situ (DCIS), 11 invasive lobular carcinoma, 2 malignant phyllodes tumor, and 14 others (Table 2). The mean size of the benign lesions was 34.0 mm (from 5 to 110 mm) and that of malignant lesions was 36.8 mm (from 7 to 60 mm).

MRI protocol: MRI was performed with a General Electric (GE) Signa CV/i 1.5T ver. 9.1 MRI unit equipped with a breast coil (surface coil). Prior to DWI, fast recovery fast spin echo (FRFSE) with CHESS was performed for fat saturation in the sagittal plane. After DWI was performed in the axial plane, 3 dimensional fast spoiled gradient recalled acquisition in the steady state (3DFSPGR) with Spec IR for fat saturation in the sagittal plane was performed before and after administration of gadopentetate dineglumine (0.2 mmol/kg). Subtraction images were produced with 3DFSPGR for identification of enhancement. 2DFSPGR with CHESS in the axial plane was performed after enhancement. Imaging parameters were as follows: 2DFRFSE (TR 3000, eff TE 85, 256 × 192, 3NEX), DWI [spin echo-single shot echo planar image (EPI) and motion probing gradient (MPG) were applied along the X, Y and Z axes (isotopic DWI) before and after the 180° pulses to obtain the images used for synthesizing isotropic images; b-values were 0 and 750 s/mm^2, TR/TE: 5000/61.8, image matrix: 128 × 128, field of view: 320 × 240 mm, slice thickness: 6 mm, spacing: 1 mm, 5NEX, acquisition time: 100 s], 3DFSPGR (TR 5.7, TE 1.2, flip angle: 20°, image matrix: 256 × 160, 2NEX), 2DFSPGR (TR 200, TE minimum, flip angle: 90°, image matrix: 512 × 192, 3NEX).

ADC value: All ADC values were calculated according to the formula: $ADC = -(1/b)\ln(S/So)$, where So and S are the signal intensities in the region of interest (ROI), obtained with different gradient factors (b values of 0, 750, and 1000

Table 3. Categorization of the four groups of correlation between low ADC value distribution on the ADC map and tumor distribution in the pathologic figures

Group	Distribution of Low ADC Values on ADC Map	n	%
G-1	Accurate distribution	129	77
G-2	Overestimation	15	9
G-3	Underestimation	11	7
G-4	False negative	12	7
Total		167	

G-1: Low ADC area similar to tumor distribution
G-2: Low ADC area greater than tumor distribution
G-3: Low ADC area smaller than tumor distribution
G-4: No decline in ADC

s/mm^2). ADC distribution was demonstrated on an ADC color map created with Advantage Workstation ver. 4.0 (GE). The ROI was placed in the target lesion and normal breast area on the ADC map with reference to subtraction images originating from 3DFSPGR and 2DFSPGR imaging after enhancement. The ROIs of the tumor lesions were smaller than the mass size excluding the normal tissue area. The size of the ROI in the area of normal breast tissue was 10 mm in diameter. Each ROI was positioned twice with a change of location and ADC values were averaged.

ADC values of benign lesions, malignant lesions, and normal breast tissues were compared, as were those of non-invasive ductal carcinoma (NIDC) and invasive ductal carcinoma (IDC). NIDC was considered to include predominant NIDC.

On the subject of malignant cases, we determined a low ADC value for malignant lesions as being less than 1.6×10^{-3} mm^2/s. We recognized the low ADC value area by a certain color on the ADC map and compared ADC maps with pathological figures to determine the accuracy of the ADC map for cancer extension. We categorized the pattern of correlation between the distribution of ADC values on the ADC map and the cancer extension in the pathological figure into 4 groups: Group 1 (G-1), where the area of low ADC values was almost the same as the tumor extension; Group 2 (G-2), where the area of low ADC values was wider and more than twice the area of tumor extension; Group 3 (G-3), where the area of low ADC values was smaller and less than one-half the area of tumor extension; and Group 4 (G-4), where no ADC reduction was observed (Table 3).

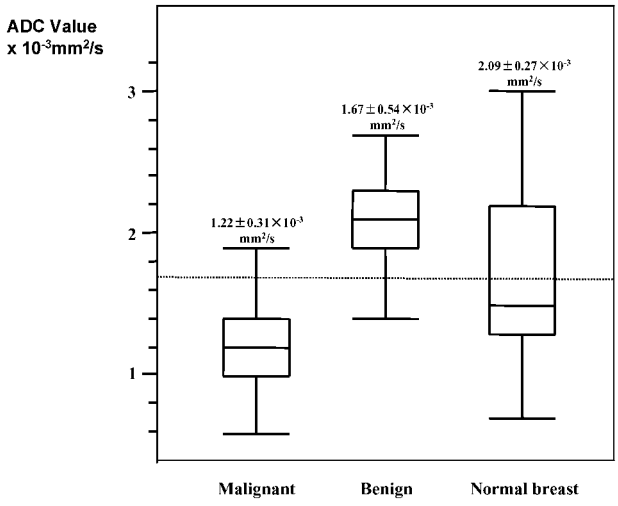

Fig. 1. Comparison among ADC values for malignant lesions, benign lesions, and normal breast tissues

Statistics

Tukey-Kramer's honesty significant difference (HSD) test was used to compare the mean ADC values of malignant tumor, benign tumor, and normal breast tissue.

The Wilcoxon signed rank sum test was used to analyze differences in the mean ADC value for significance between IDC and NIDC or predominant NIDC.

Result

Comparison of ADC values: The mean ADC value of the 167 malignant lesions was $1.22 \pm 0.31 \times 10^{-3}$ mm^2/s (ranging from 0.6 to 2.7×10^{-3} mm^2/s). The mean ADC value of the 24 benign lesions was $1.67 \pm 0.54 \times 10^{-3}$ mm^2/s (ranging from 0.7 to 3.0×10^{-3} mm^2/s), and the mean ADC value of normal breast tissue in all cases was $2.09 \pm 0.27 \times 10^{-3}$ mm^2/s (ranging from 1.4 to 3.0×10^{-3} mm^2/s). A statistically significant difference in ADC values was observed between benign tumors, malignant tumors, and normal breast tissues (Fig. 1).

The mean ADC value of IDC was $1.20 \pm 0.32 \times 10^{-3}$ mm^2/s and that of NIDC was $1.35 \pm 0.25 \times 10^{-3}$ mm^2/s. There was also significant difference ($p = 0.02$) between them (Fig. 2).

Sensitivity and specificity of ADC value: With an ADC value of less than 1.6×10^{-3} mm^2/s defined as being an indicator of malignancy, 155 of the 167 malignant cases were identified as malignant lesion on the ADC map without concern for the range of ADC reduction. Sensitivity to malignant lesions was 93%. On the other hand, 13 benign cases were

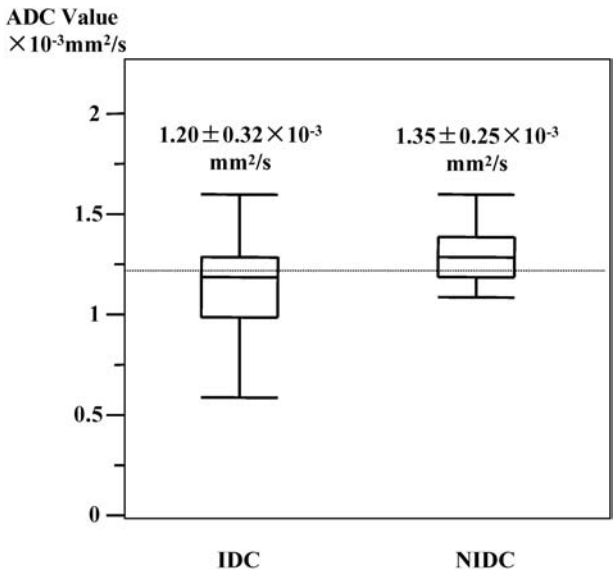

Fig. 2. Comparison between ADC values of NIDC and IDC

misdiagnosed as malignant lesions. Thus, the specificity was 46% (11/24) and the accuracy was 87% (166/191).

In 13 cases, benign lesions were misdiagnosed. The histologic details of these benign lesions were as follows: five cases of intraductal papilloma with a mean ADC value of 1.24×10^{-3} mm^2/s (ranging from 0.9 to 1.4×10^{-3} mm^2/s); three cases of fibroadenomatosis, one of ductal hyperplasia, and one of sclerosing adenosis with a mean ADC value of these lesions, fibrocystic change of 1.34×10^{-3} mm^2/s (ranging from 1.2 to 1.5×10^{-3} mm^2/s); two cases of fibroadenoma with a mean ADC value of 1.1×10^{-3} mm^2/s; and one case of granuloma with an ADC value of 0.7×10^{-3} mm^2/s.

Comparison of ADC map and histopathologic features: All malignant cases were classified into 4 groups according to the concurrence of tumor extension and distribution of low ADC values on the ADC map. A total of 129 cases were classified as G-1; 15 cases as G-2; 11 cases as G-3; and 12 cases as G-4 (Table 3).

Of the cases categorized as G-1, 11 cases represented a small compartment of DCIS foci neighboring the main tumors, which DWI did not depict. While these lesions were in the same segment as the main tumors and the sizes were less than one half as large as the main tumors, we decided to categorize such cases as G-1 (Fig. 3).

Regarding G-2, the histopathologic details of the overdiagnosed area, which showed a low ADC value of less than 1.6×10^{-3} mm^2/s instead of an absence of malignant compartment, were as follows: 1 case of apocrine metaplasia; 7 of ductal or lobular hyperplasia; 2 of blunt duct adenosis; 2 of sclerosing adenosis; 1 of fibroadenomatosis; and 2 no evidence of malignancy (Fig. 4).

With regard to G-3, the histopathologic details of the malignant component, where the ADC map did not show a low ADC value, were as follows: 4 cases showed comedo-type DCIS containing notable bleeding and necrosis, 1 case was an intracystic papillary carcinoma, 1 case showed sporadic DCIS and lobular carcinoma invasion, 2 cases were necrosis and hemorrhage section of phyllodes malignant, 2 cases were marginal zone of lobular carcinoma, and 1 case was papillotubular carcinoma. In other words, 7 cases had bleeding component in G-3. In addition, 2 cases of lobular carcinoma and 1 case of lobular carcinoma with DCIS showed sparse and small foci of tumor components in the area which the ADC map did not depict as a low ADC area (Fig. 5).

The histologic details of G-4 were as follows: 3 cases of DCIS, 2 of scirrhous carcinoma, 2 of solid tubular carcinoma, 2 of papillotubular carcinoma, and 1 each of intracystic papillary carcinoma, malignant phyllodes tumor, and mucinous carcinoma. In these cases, some notable histologic characters were seen in the specimens. Nine cases showed remarkable blood components in the specimens of malignant components (Fig. 6). In G-3 and G-4, 14 cases out of 16 with bloody components showed as high-intensity lesions in T_1-weighted images.

Discussion

According to the past reports, MRI has been confirmed as an essential tool for examination of the breasts because of its remarkably higher sensitivity with the use of enhancement material for breast carcinoma than that of ultrasound and mammography. MRI demonstrates its virtues in the research of occult cancers, where mammography and ultrasound can neither detect nor assess the cancer extension. Preoperative contrast-enhanced MRI of the breast has the potential to reveal mammographically and sonographically hidden multifocal breast carcinoma.[16–26] However, the disadvantages of MRI compared with mammography and ultrasound are the long scan times, usually 20 to 30 min, and the need for a contrast medium. In addition, the contrast material increases the cost. Furthermore, we feel that the conventional diagnostic techniques of breast MRI, morphological diagnosis and analysis of dynamic enhancement patterns, are limited to a certain degree.[27–29] On the other hand, DWI reflects some elements that affect proton diffusion, for example

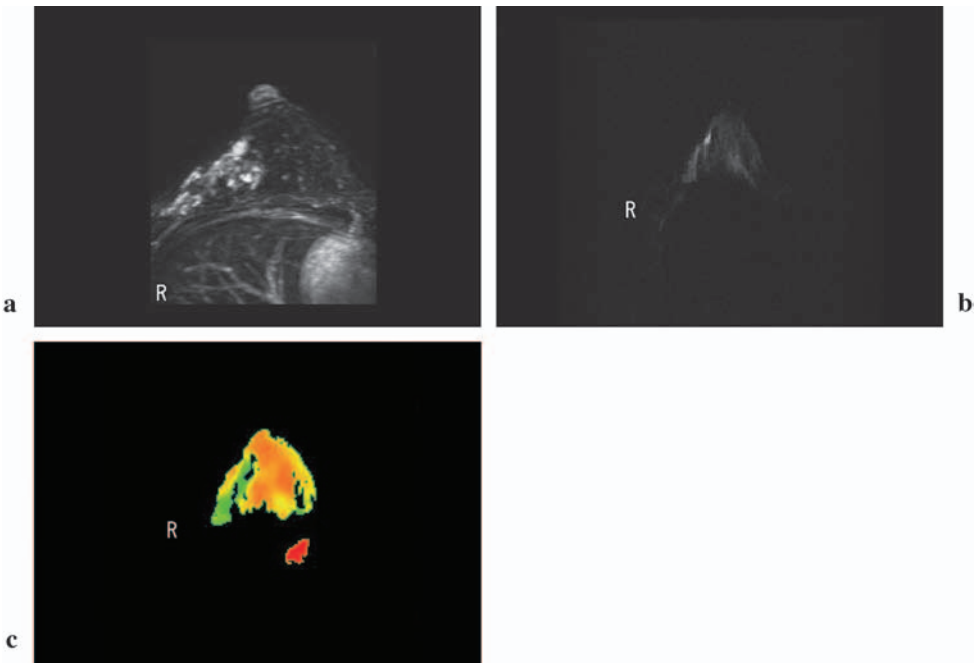

Fig. 3. A case of ductal carcinoma *in situ*
a: Maximum intensity projection (MIP) image of subtraction image obtained with 3DFSPGR. The segmental nodular enhancement is displayed in area C.
b: DWI in the axial plane shows a segmental high-intensity lesion in area C.
c: An ADC map of the same level as Fig. 3b. The greenish color indicates a low ADC value. The distribution of low ADC values corresponds to the enhancement lesion of MIP image on Fig. 3a.

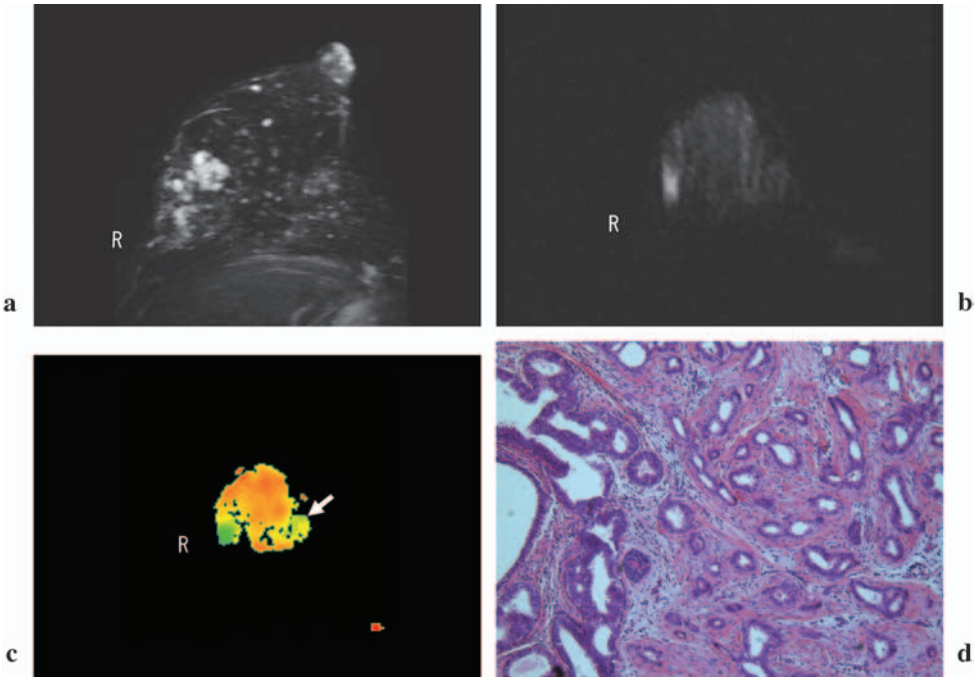

Fig. 4. A case of scirrhous carcinoma
a: MIP of subtraction image obtained with 3DFSPGR. The enhanced mass lesion in area C indicates a primary mass lesion. Note the diffuse scattering of small enhanced nodules in the mammary gland.
b: DWI reveals a high-intensity lesion in area C as a 3DFSPGR image.
c: An ADC map of the same level as Fig. 4b. The primary mass lesion shows a low ADC value. Area A also shows a low ADC region (white arrow).
d: Pathologic figure of area A. The sclerosing adenosis is prominent (H&E, ×40).

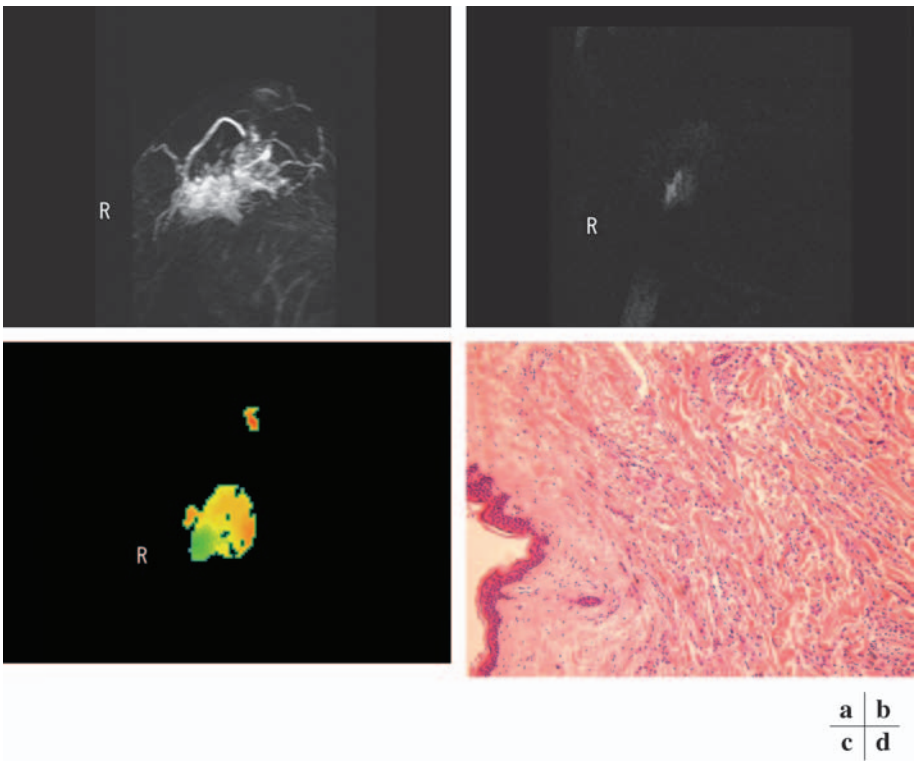

Fig. 5. A case of invasive lobular carcinoma
a: A MIP image of a subtraction image shows a speculated enhanced mass lesion extending from area A to area C. Some linear and nodular enhancements extend to the nipple site, which suggest tumor invasion.
b: DWI reveals a localized high-intensity lesion in area C that is smaller than the enhanced lesion in the 3DFSPGR image.
c: A low ADC area is evident in area C. The extending enhanced lesion obtained with 3DFSPGR is not visualized on the ADC map.
d: Histologic appearance of the area where the 3DFSPGR image shows enhancement, whereas the ADC map did not show ADC reduction (H&E, ×100). Sparse and scattered distribution of cancer cells is evident in the stroma.

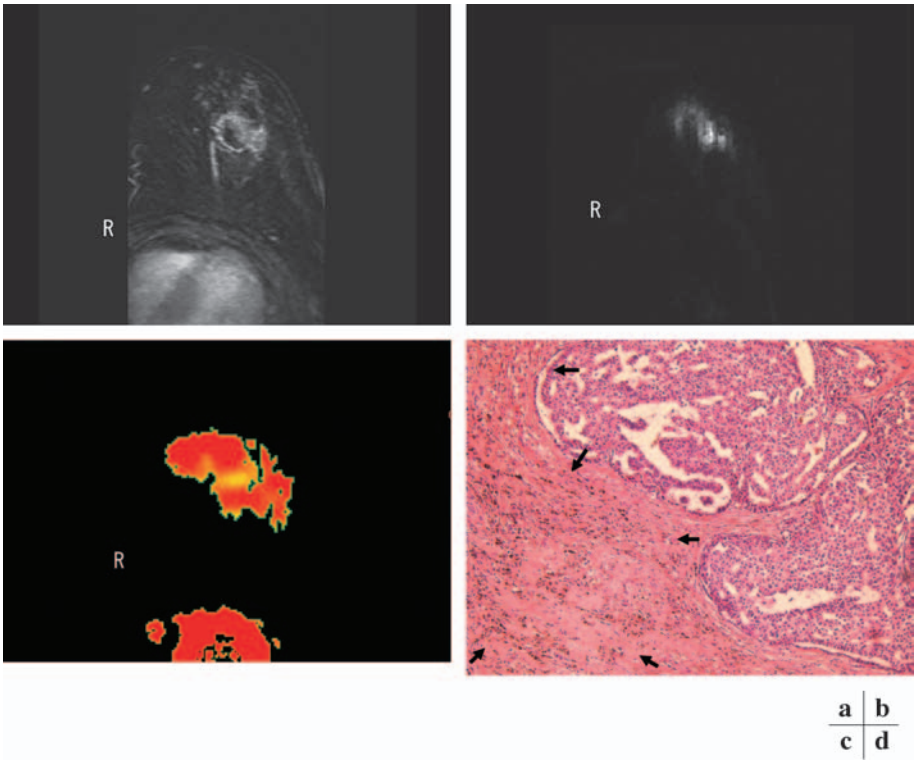

Fig. 6. A case of intracystic papillary carcinoma surrounded by intraductal carcinoma
a: A cystic mass lesion in area D. The irregular mass along the wall of the cystic mass protrudes inward. Some nodular enhancement is evident around the cystic mass lesion.
b: DWI of the same level as that of Fig. 5a. The high-intensity lesion of DWI corresponds approximately to the 3DFSPGR image.
c: ADC map of the same level as that of Fig. 5b. The low ADC area is absent.
d: The histopathologic figure neighboring the lesion of intracystic papillary carcinoma shows hemosiderine-laden macrophage surrounding the intraductal carcinoma component (black arrow; H&E, ×40).

cell density, tumor structure, intestinal structure, and tissue components such as edema, necrosis, and fibrosis. With regard to breast DWI, a high sensitivity to breast malignant tumor has been already proven. Y. Guo demonstrated 93% sensitivity with the threshold of 1.3×10^{-3} mm^2/s of ADC value for breast cancer, while Y. Kuroki et al. showed statistically lower ADC values for breast carcinomas than those of benign tumors.[3,15] Our study showed a 93% sensitivity to malignant tumors among the G-1, G-2, and G-3 cases, with a threshold of 1.6×10^{-3} mm^2/s of ADC value. As

for the false negative cases and underestimated cases, in which the ADC values were not decreased in the carcinoma components, notable histopathologic characteristics were observed in the specimens, specifically necrosis and hemorrhage. Seven cases of G-3 and 9 cases of G-4 showed hemorrhage or necrosis mainly owing to DCIS or malignant phyllodes tumor. Conversely, hemorrhage was also observed in some specimens of intraductal papilloma. However, most intraductal papilloma showed low ADC values. The reason for this anomaly is unknown. We speculate that the character of the hemorrhage differs between the malignant tumors and intraductal papilloma. Comedo-type DCIS show the phenomenon of necrosis, hemorrhage, and calcification. We hypothesize that the high degree of oxidation as a consequence of necrosis affects the high ADC value. Specifically, the strong effect of magnetic susceptibility is one mechanism of high ADC values in DCIS and malignant phyllodes tumor with bleeding. Since seven of the bleeding cases showed high intensity in T_1-weighted images, it is possible to speculate about the occurrence of hemorrhage by referring to other sequences.

In 3 cases categorized as G-3, scattering and sparse distribution of lobular carcinoma and DCIS did not represent low ADC values. Moreover, with respect to 11 cases categorized as G-1 in which the ADC map did not show low values in DCIS around main tumors, one reason for the misdiagnosis is the limited spatial resolution of DWI. However, the sensitivity to small foci and the sparse distribution of tumor will improve with advances in the spatial resolution of DWI.

As for benign lesions, although Guo et al. showed all fibroadenoma were correctly diagnosed as benign lesions, one case of duct ectasia and one of intraductal papilloma were incorrectly categorized.[3] In our study, specificity was markedly low. Most cases of intraductal papilloma and more than half the cases of fibrocystic disease showed low ADC values and were categorized as malignant lesions. Moreover, benign proliferative changes such as ductal hyperplasia, fibroadenosis, and lobular hyperplasia around the carcinoma have resulted in over-estimation of cancer extension. Some pathogenesis of this phenomenon can be considered. Guo et al. confirmed the relation between ADC values and cell density, which exhibited an inverse proportion. Fibrocystic disease sometimes shows a high cell density and inflammatory reactions. This phenomenon restricts proton diffusion, a possible reason for low ADC values. However, the disparity between the ADC values of fibrocystic disease and malignancy could be divided further with a higher b-value. This is because the effect of perfusion is smaller at higher b-values and the reduction in ADC values of malignant lesions is more prominent than that of benign lesions due to angiogenesis of malignant tumor.[16,30] Only two cases of fibroadenoma were found in our study, both of the pericanalicular type, and both exhibited low ADC values. Although Guo et al. did not mention the detailed type of fibroadenoma, it is possible that not all fibroadenoma will show high ADC values. Therefore, ADC values are still unreliable for fibrocystic disease, intraductal papilloma, and some types of fibroadenoma. As our study showed low specificity, DWI is still insufficient for qualitative diagnosis.

Conclusion

Our trial sought to verify the usefulness of breast DWI in clinical applications. We discovered that the sensitivity is sufficient for detecting malignant lesions. In addition, with DWI we were able to obtain images with one-minute scan times. This satisfies the requirements for screening use. This study demonstrated the potential for DWI to be used in the assessment of cancer extension. The spatial resolution and accuracy of differentiation will be improved with advances in MRI technology.

References

1. Filippi M, Cercignani M, Inglese M, et al. Diffusion tensor magnetic resonance imaging in multiple sclerosis. Neurology 2001; 56:304–311.
2. Bammer R. Basic principles of diffusion-weighted imaging. Eur J Radiol 2002; 45:169–184.
3. Guo Y, Cai YQ, Cai ZL, et al. Differentiation of clinically benign and malignant breast lesions using diffusion-weighted imaging. J Magn Reson Imaging 2002; 16:172–178.
4. Lyng H, Haraldseth O, Rofsrad EK. Mesurement of cell density and necrotic fraction in human melanoma xenografts by diffusion weighted magnetic resonance imaging. Magn Reson Med 2000; 43:828–836.
5. Warach S, Boska M, Welch KM. Pitfalls and potential of clinical diffusion-weighted MR imaging in acute stroke. Stroke 1997; 28:481–482.
6. Noguchi K, Watanabe N, Nagayoshi T, et al. Role of diffusion-weighted echo planar MRI in distinguishing between brain abscess and tumour: a preliminary report. Neuroradiology 1999; 41:171–174.
7. Tsuruda JS, Chew WM, Moseley ME, et al. Diffusion-weighted MR imaging of the brain: value of differentiating between extraaxial cysts and

epidermoid tumors. AJNR Am J Neuroradiol 1990; 11:925–931.
8. Kim T, Murakami T, Takahashi S, et al. Diffusion weighter single-shot echoplanar MR imaging for liver disease. AJR Am J Roentgenol 1999; 173: 393–398.
9. Namimoto T, Yamashita Y, Sumi S, et al. Focal liver masses: characterization with diffusion-weighted echo planar MR imaging. Radiology 1997; 04:739–744.
10. Kuroki S, Nasu S, Murakami K, et al. Pancreatic cancer on DWI. Nippon Acta Radiol 2003; 63: S184.
11. Moteki T, Ishizaka H, Horikoshi H, et al. Differentiation between hemangiomas and hepatocellular carcinomas with the apparent diffusion coefficient calculated from turboFLASH MR images. JMR 1995; 5:187–191.
12. Moteki T. Ishizaka H. Diffusion-weighted EPI of cystic ovarian lesions: evaluation of cystic contents using apparent diffusion coefficients. J Magn Reson Imaging 2000: 12:1014–1019.
13. Maier CF, Paran Y, Bendel P, et al. Quantitative diffusion imaging in implanted human breast tumors. Magn Reson Med 1997; 37:576–581.
14. Englander SA, Ulug AM, Brem R, et al. Diffusion imaging of human breast. NMR Biomed 1997; 10:348–352.
15. Kuroki Y, Katsushiro N, Kuroki S, et al. Diffusion-weighted imaging of breast cancer with the sensitivity encoding technique: analysis of apparent diffusion coefficient value. MRMS 2004; 3:79–85.
16. Buadu LD, Murakami J, Murayama S, et al. Breast lesions: correlation of contrast medium enhancement patterns on MR images with histopathologic findings and tumor angiogenesis. Radiology 1996; 200:639–649.
17. Mumtaz H, Hall-Craggs MA, Davidson T, et al. Staging of symptomatic primary breast cancer with MR imaging. AJR Am J Roentgenol 1997; 169: 417–424.
18. Morris EA, Schwartz LH, Dershaw DD, et al. MR imaging of the breast in patients with occult primary breast carcinoma. Radiology 1997; 205:437–440.
19. Boné B, Péntek Z, Perbeck L, et al. Diagnostic accuracy of mammography and contrast-enhanced MR imaging in 238 histologically verified breast lesions. Acta Radiol 1997; 38:489–496.
20. Stomper PC, Winston JS, Herman S, et al. Angiogenesis and dynamic MR imaging gadolinium enhancement of malignant and benign breast lesions. Breast Cancer Res Treat 1997; 45:39–46.
21. Boetes C, Barentsz JO, Mus RD, et al. MR characterization of suspicious breast lesions with a gadolinium-enhanced turbo FLASH subtraction technique. Radiology 1994; 193:777–781.
22. Heiberg EV, Perman WH, Herrmann VM, et al. Dynamic sequential 3D gadolinium-enhanced MRI of the whole breast. Magn Reson Imaging 1996; 14:337–348.
23. Baum F, Fischer U, Vosshenrich R, et al. Classification of hypervascularized lesions in CE MR imaging of the breast. Eur Radiol 2002; 12:1087–1092.
24. Fischer U, Kopka L, Grabbe E. Breast carcinoma: effect of preoperative contrast-enhanced MR imaging on the therapeutic approach. Radiology 1999; 13:881–888.
25. Orel SG, Schnall MD, Powell CM, et al. Staging of suspected breast cancer: effect of MR imaging and MR-guided biopsy. Radiology 1995; 196:115–122.
26. Rieber A, Merkle E, Böhm W, Brambs H-J, Tomczak R. MRI of histologically confirmed mammary carcinoma: clinical relevance of diagnostic procedures for detection of multifocal or contralateral secondary carcinoma. J Comput Assist Tomogr 1997; 21:773–779.
27. Boetes C. Strijk SP. Holland R. et al. False-negative MR imaging of malignant breast tumors. Eur Radiol 1997; 7:1231–1234.
28. Cohen EK, Leonhardt CM, Shumak RS, et al. Magnetic resonance imaging in potential postsurgical recurrence of breast cancer: pitfalls and limitations. Can Assoc Radiol J 1996; 47:171–176.
29. Liu PF. Debatin JF. Caduff RF, et al. Improved diagnostic accuracy in dynamic contrast enhanced MRI of the breast by combined quantitative and qualitative analysis. Br J Radiol 1998; 71:501–509.
30. Hulka CA, Smith BL, Sgroi DC, et al. Benign and malignant breast lesions: differentiation with echoplanar MR imaging. Radiology 1995; 197:33–38.